Electronic Supplementary Material (ESI) for Soft Matter.

Supplementary Information

Sliding Friction of a Pillar Array Interface: Part I

S.1 Micropillar friction data (RT-RT)

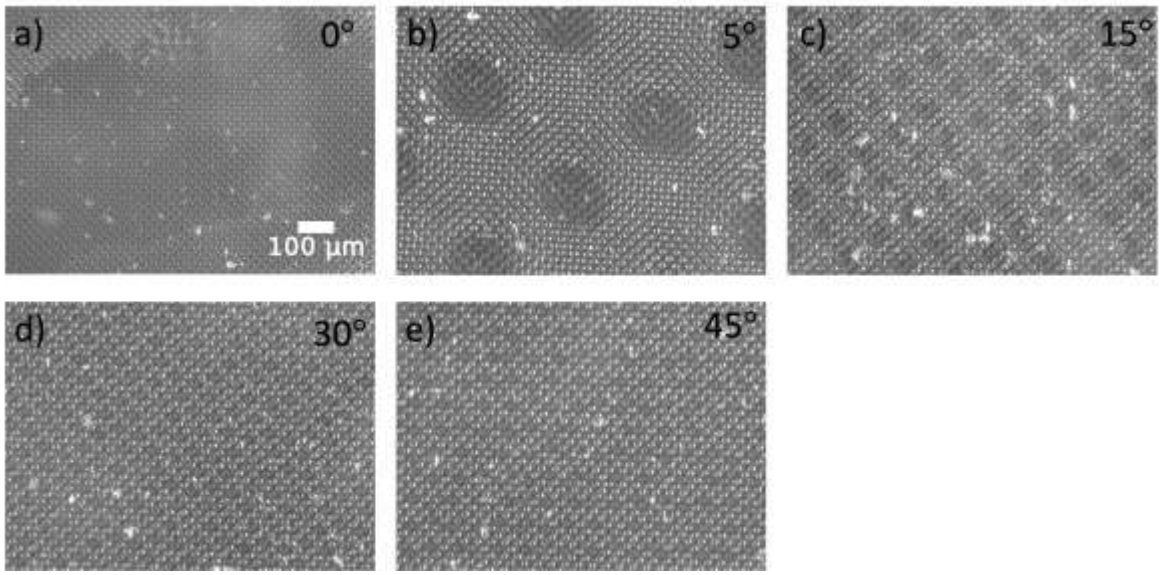

Figure S1. Interfacial screw dislocations
Interfacial dislocations between micropillar samples at $\lambda = 1$ for different misorientations θ. a) θ=0° b) θ=5° c) θ=15° d) θ=30° e) θ=45°.

Figure S1 shows the interface for samples with $\lambda = 1$ ($no\ lattice\ parameter\ mismatch$) as they come in contact and before sliding. $\lambda = 1$ means both the samples have same interpillar spacing and are cured at room temperature (RT-RT). Fig. S1a shows the case of $\lambda = 1$ and misorientation, θ = 0°. Ideally there should be no dislocations because there is no mismatch, but edge nucleated dislocations [1] are seen to pass through the interface during sliding (video: **V1_lambda=1_0_deg.avi.** For a misorientation of 5° (Fig. S1b), an array of screw dislocations is formed, and density of dislocations increases as we increase the misorientation between two samples as seen in Fig S1 a) to e). Figures S1c, S1d and S1e show an array of screw dislocations at misorientation angles, $\theta = 15°, 30°$ & 45°, respectively. The video for screw dislocation with $\lambda = 1$ and $\theta = 5°$ is **V3_lambda=1_5_deg_ ScrewDislocation.avi.**

Figure S2 a) to e) below shows shear stress versus displacement plots for pillar samples with $\lambda = 1$ and different misorientations θ from $0°\ to\ 45°$.

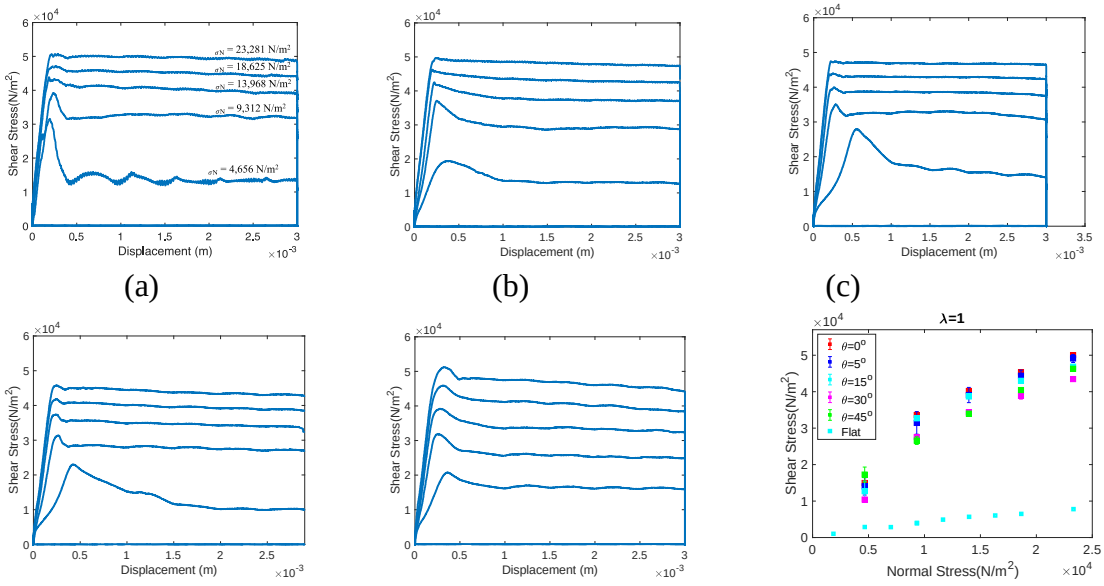

Figure S2. $\lambda = 1$: This figure presents friction data for $\lambda = 1$ at various misorientations $\theta = 0°, 5°, 15°, 30°$ & $\theta = 45°$ and normal loads from 4,656 N/m^2 to 23,281 N/m^2. (a) Friction stress vs shear displacement for $\theta = 0°$ for normal load varying from 4,656 N/m^2 to 23,281 N/m^2 (b) $\theta = 5°$ (c) $\theta = 15°$ (d) $\theta = 30°$ (e) $\theta = 45°$ (f) Friction stress vs normal stress for $\lambda = 1$ and at various misorientations $\theta = 0°, 5°, 15°, 30°$ & $\theta = 45°$ and normal load varying from 4,656 N/m^2 to 23,281 N/m^2.

S.2 Micropillar Friction data 60-RT and 110-RT

Figure S3 shows arrays of dislocations on the interface at different orientation mismatch and different lattice mismatch for λ=1.006±0.001. Here, 60-RT means that one of the samples is cured at 60℃ and the other is cured at room temperature (RT). Fig S3a shows an image for edge dislocations and Fig S3b shows mixed dislocations where λ=1.006±0.001 and θ = 5°. Figures S3 c) to e) show mixed dislocations for λ=1.006 at θ = 15°, θ = 30° and θ = 45° respectively.

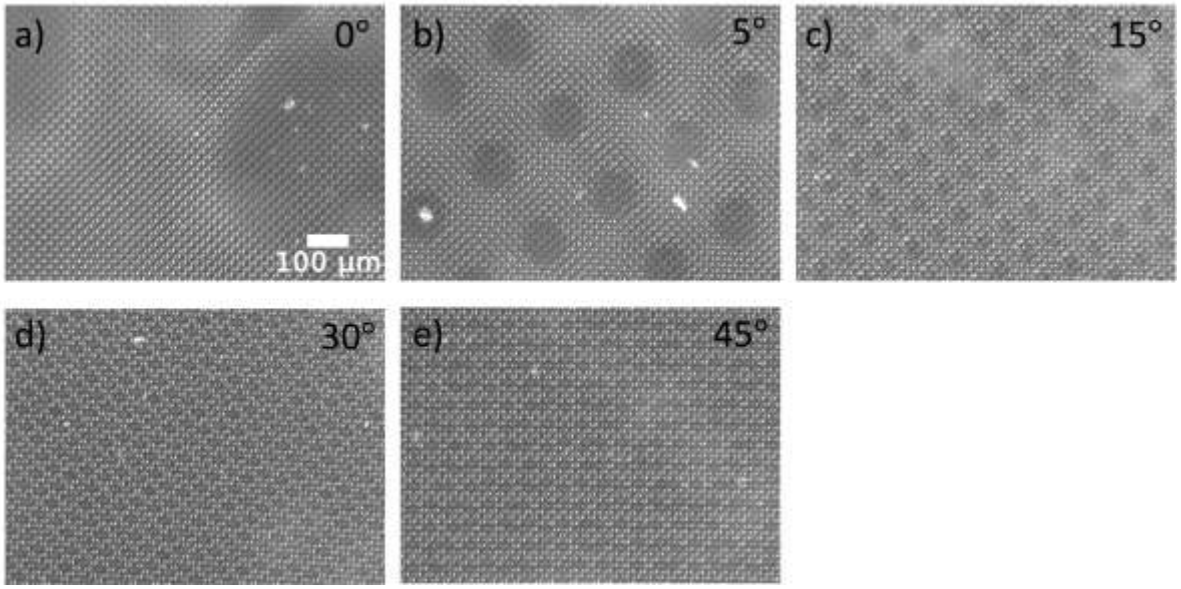

Figure S3 $\lambda = 1.006$: Interfacial dislocations
Interfacial dislocations between micropillar samples at $\lambda = 1.006$ at different orientations, θ. a) θ=0° b) θ=5° c) θ=15° d) θ=30° e) $\theta = 45°$.

Figure S4 shows shear stress data for pillar sample with different lattice spacing with $\lambda = 1.006$. Each experiment is performed at certain $\lambda, and\ \theta$ values at normal loads 4656 N/m^2 to 23000 N/m^2. Each experiment shows friction stress depends on normal load and increases at normal load is increased. Figures S4 a) to e) show shear stress vs displacement for $\lambda = 1.006$ for $\theta = 0°$, $\theta = 5°$, $\theta = 15°$, $\theta = 30°$, $\theta = 45°$ respectively. Figure S4 f) shows friction stress versus normal stress for $\lambda = 1.006$ at different values of θ and normal stress.

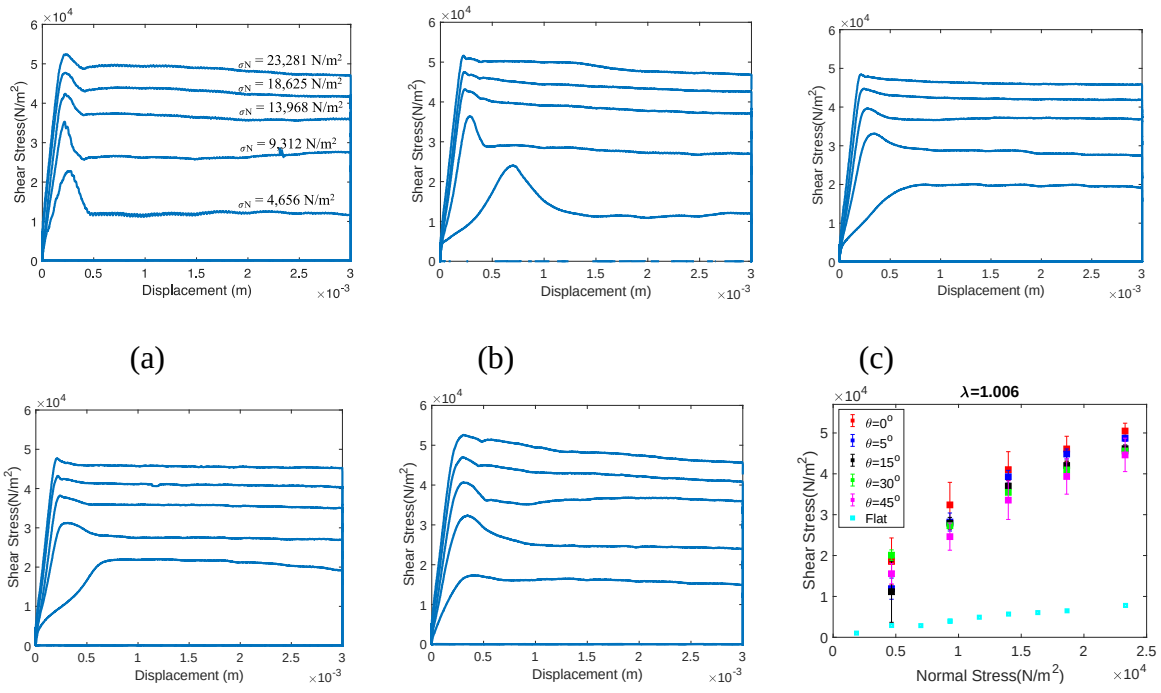

Figure S4 $\boldsymbol{\lambda = 1.006}$: Friction data for $\lambda = 1.006$ at various misorientations $\theta = 0°, 5°, 15°, 30° \& 45°$. (a) Friction stress vs shear displacement for $\theta = 0°$ for normal load varying from 4,656 N/m^2 to 23,281 N/m^2 (b) $\theta = 5°$ (c) $\theta = 15°$ (d) $\theta = 30°$ (e) $\theta = 45°$. (f) Friction stress vs normal stress for $\lambda = 1.006$ and at various misorientations $\theta = 0°, 5°, 15°, 30° \& 45°$ and normal load varying from 4,656 N/m^2 to 23,281 N/m^2.

Figures S5 and S6 shows results from a set of experiments is performed for a 110-RT sample i.e., lattice mismatch $\lambda=1.023\pm0.001$ and at various misorientations. Here, 110-RT means that one of the samples is cured at 110℃ and the other one is cured at room temperature (RT). The interface of two samples shows an array of edge and screw dislocations. In the first case (Fig. S5a) where $\lambda=1.023\pm0.001$, $\theta = 0°$, an array of edge dislocations is formed. As the misorientation angle, θ, is further increased to $5°, 15°, 30° \& 45°$, arrays of mixed dislocations are subsequently formed as shown in figures S5 b) to e). And, it can also be seen from the figures, that if misorientation angle is increased, the density of dislocations increases[1]. Figures S6 a) to e) show variation of shear stress vs shear displacement at different misorientations from S6 a) to S6 e). Figure S6 f) shows variation of shear stress with normal stress when $\lambda=1.023$ and is performed for various misorientations, $\theta= 0°, 5°, 15°, 30° \& 45°$ and normal stresses.

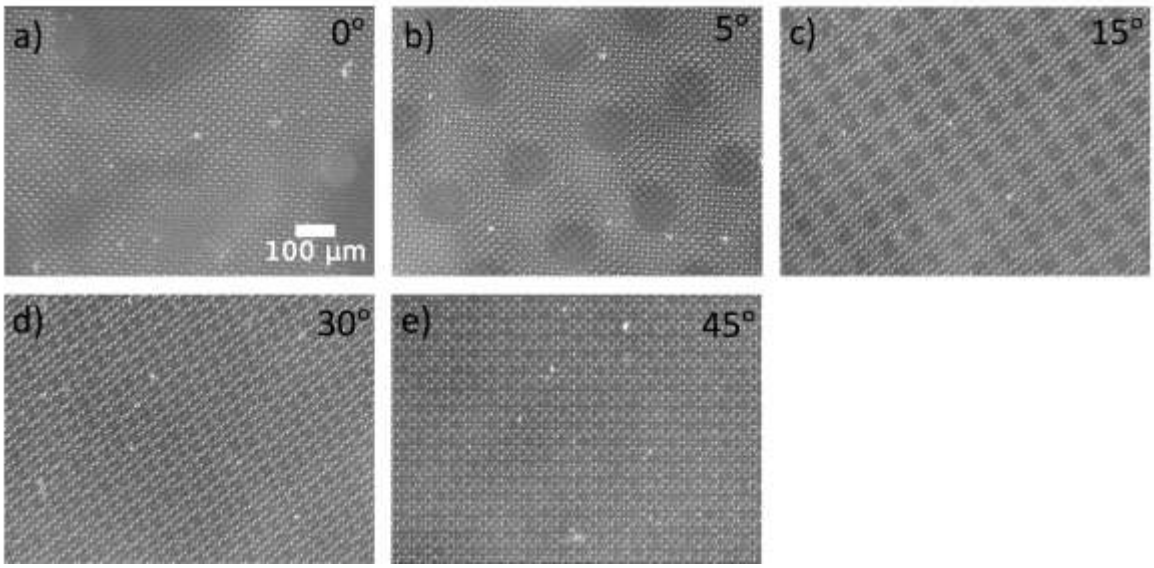

Figure S5: $\lambda = 1.023$ Interfacial dislocations

Interfacial dislocations between micropillar samples at $\lambda = 1.023$ at different orientations. a) θ=0°, b) θ=5°, c) θ=15°, d) θ=30°, (e) θ=45°.

This video shows an experiment for $\lambda = 1.023$ and $\theta = 0°$, **V8_lambda=1.023_0deg_EdgeDislocation**

This video shows an experiment for $\lambda = 1.023$ and θ=5°, showing mixed dislocations with character of both an edge and a screw dislocation, **V10_lambda=1.023_5_deg_MixedDislocation.avi**

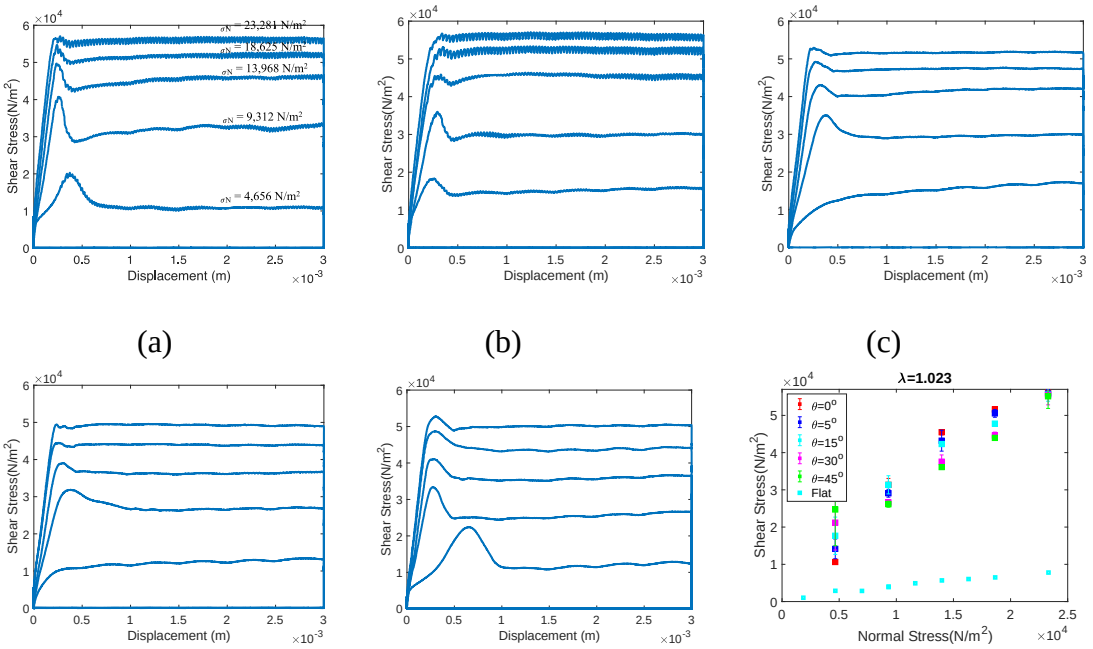

Figure S6: $\lambda = 1.023$: This figure represents friction data for $\lambda = 1.023$ at various misorientations $\theta = 0°, 5°, 15°, 30°$ & $\theta = 45°$.

(a) Friction stress vs shear displacement for $\theta = 0°$ for normal load varying from 4,656 N/m^2 to 23,281 N/m^2 (b) $\theta = 5°$ (c) $\theta = 15°$ (d) $\theta = 30°$ (e) $\theta = 45°$ (f) Friction stress vs normal stress for $\lambda = 1.023$ and at various misorientations $\theta = 0°, 5°, 15°, 30°$ & $45°$ and normal load varying from 4,656 N/m^2 to 23,281 N/m^2.

S.3 Single pillar-pair experimental data

This section shows all data for single pillar-pair experiments where shear force depends on two parameters, diametric overlap, l_x and height of contact, H_c. Figure S7 a) to e) give the variation of shear force with respect to displacement in sliding direction for several cases of diametric overlaps varied from 100 % (Fig S7 a) to 0% (Fig. S7 e) and various height to contact from 4.8 mm to 0.8 mm in gaps of 1 mm. (Video **V19_Singlefiber_4.8mm_100%O** shows single pillar sliding experiment at 100% Overlap and 4.8 mm as height of contact,**).**

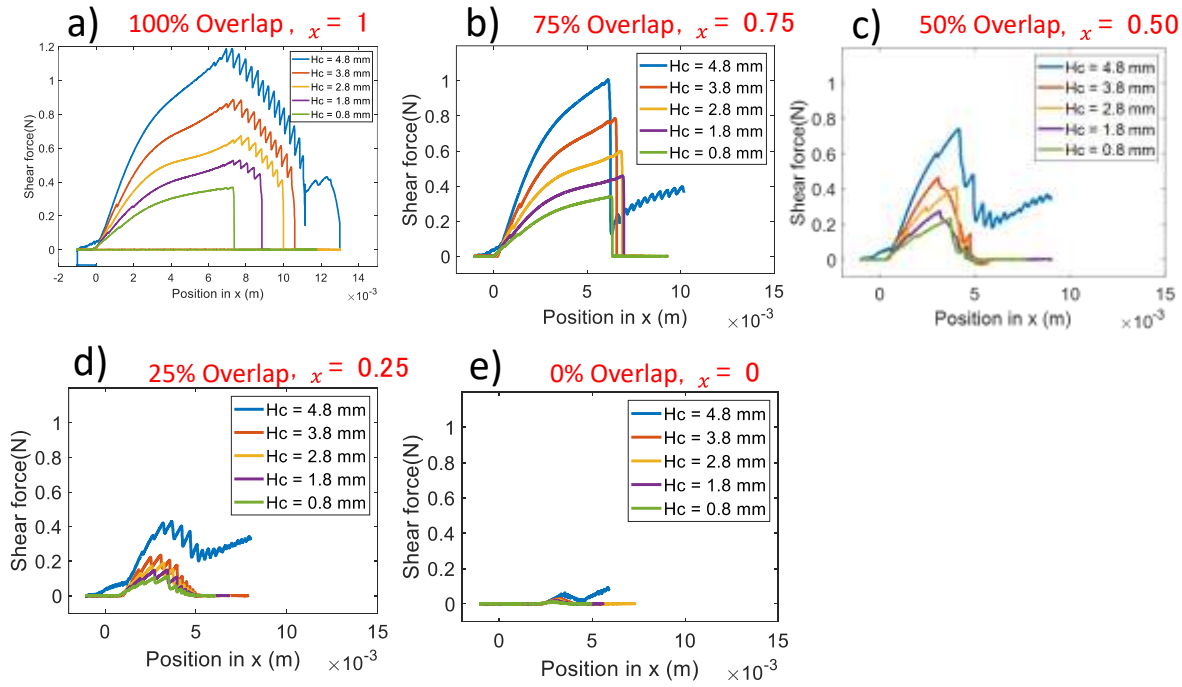

Figure S7. Single pillar experiment data: Variation of Shear force with displacement for different diametric overlaps and height of contact (H_c). (a) 100% diametric overlap ($l_x = 1$) (b) 75% ($l_x = 0.75$) (c) 50% ($l_x = 0.50$) (d) 25% ($l_x = 0.25$) (e) 0% ($l_x = 0$).

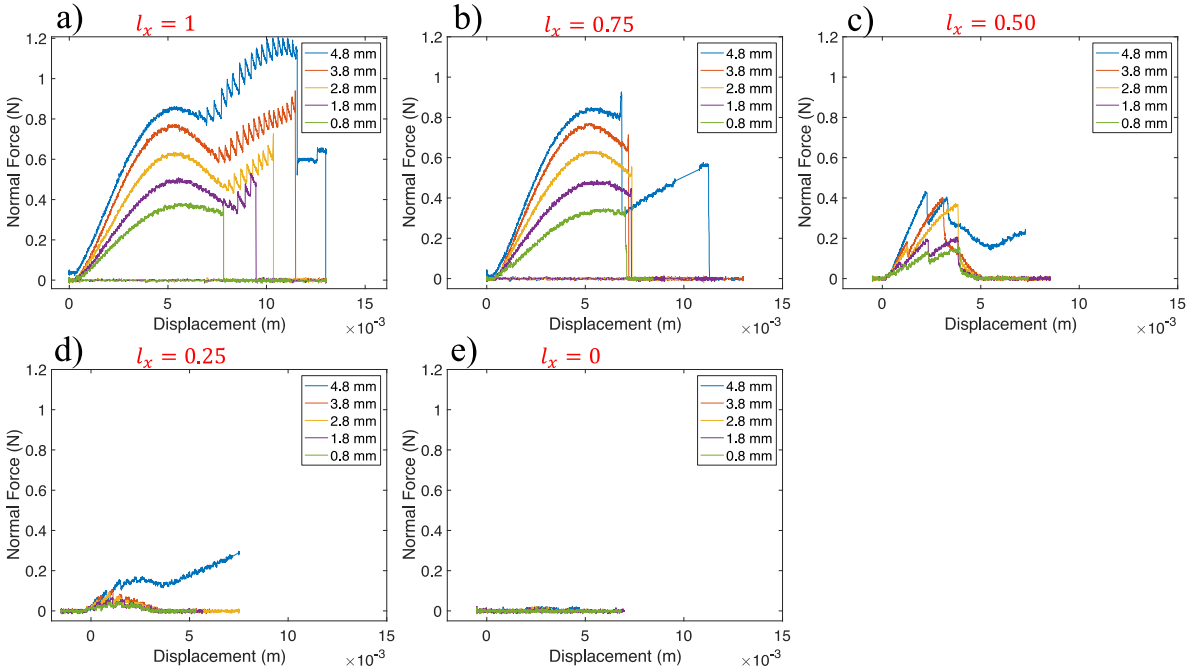

Figure S8. Single pillar experiment data: Variation of Normal force vs displacement in sliding direction for different diametric overlaps and height of contact. (a) 100% diametric overlap, $l_x = 1$ (b) $l_x = 0.75$ (c) $l_x = 0.50$ (d) $l_x = 0.25$ (e) $l_x = 0$.

Figure S8 shows variation of Normal force vs displacement in sliding direction for different diametric overlaps and height of contact. Fig S8 a) shows variation of normal force with displacement for 100% diametric overlap for different height of contact ranging from 4.8 mm to 0.8 mm in gaps of 1 mm. Similarly, figures 8 b) to 8 e) show variation of normal force with displacement for different heights of contact at diametric overlaps as 75%, 50%, 25 %, 0% respectively.

Single pillar experiments were also performed at a different aspect ratio of 2, i.e., height of pillar as 6 mm and diameter as 3 mm. Figure S9 shows variation of shear force with shear displacement for different height of contact from 6 mm to 2 mm. Figure S9 a) shows shear force variation for 100% diametric overlap. Here, shear force for maximum height of contact is less than that obtained for 4.8 mm height pillar. The more elongated pillars (6 vs. 4.8 *mm*) are more compliant. Figures S9 b) to e) show shear force versus displacement for various diametric overlaps ranging from 75% to 0%. Figure S10 shows variation of normal force for experiments in Figure S9. Figure S10 a) to e) show variation of normal force vs displacement for single pillar experiment of height 6 mm and diameter 3 mm. (Video **V20_singlefiber_6mm_100%O** shows sliding experiment of single pillars with aspect ratio = 2 and 100% diametric overlap,**).**

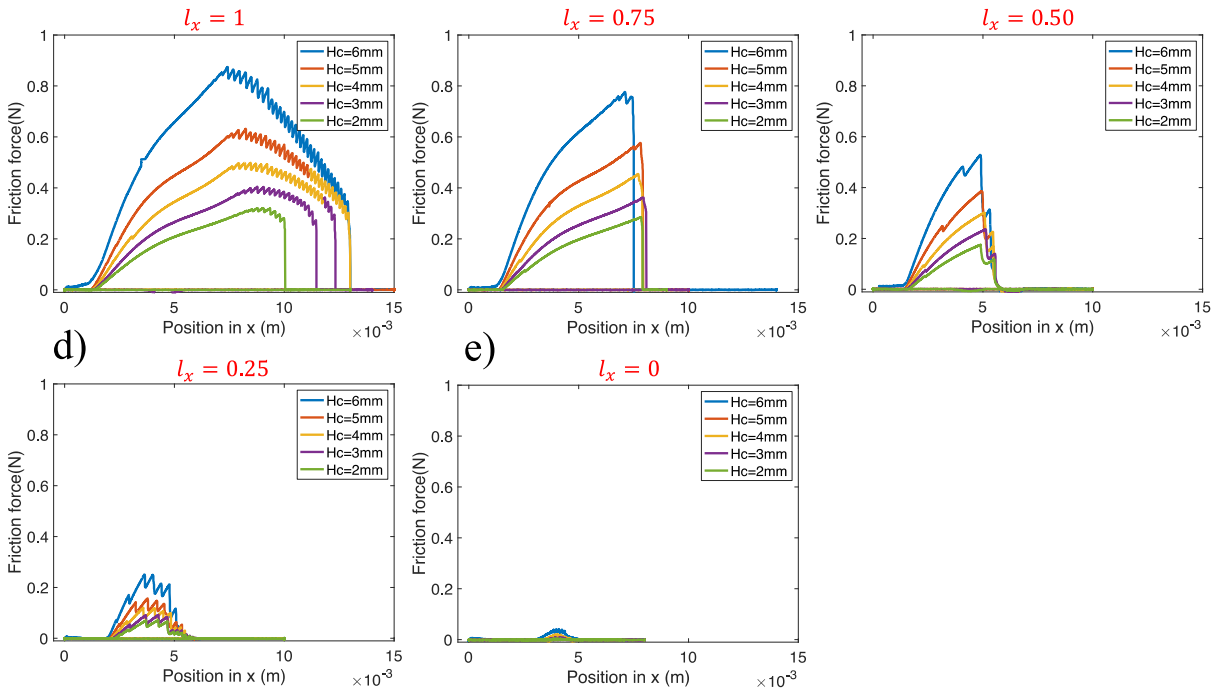

Figure S9. Single pillar data for pillar of height = 6 mm and diameter = 3 mm.
Variation of Shear force with displacement for different diametric overlaps and height of contact. (a) 100% diametric overlap, $l_x = 1$ (b) $l_x = 0.75$ (c) $l_x = 0.50$ (d) $l_x = 0.25$ (e) $l_x = 0$.

To better understand the role of adhesion forces in these single pillar-pair experiments, we also performed single pillar experiments with silicone oil as a lubricant. Figure S11 shows shear stress vs displacement for single pillar-pair experiments with lubricant. Figure S11 a) to e) shows data for different diametric overlaps from 100 % overlap to 0% overlap and height overlaps ranging from 6 mm to 2 mm in gaps of 1 mm. The lubricant barely affects the force-displacement response in the early rising part. The main difference is in the point of instability, which occurs very soon after the peak load in the shear response.

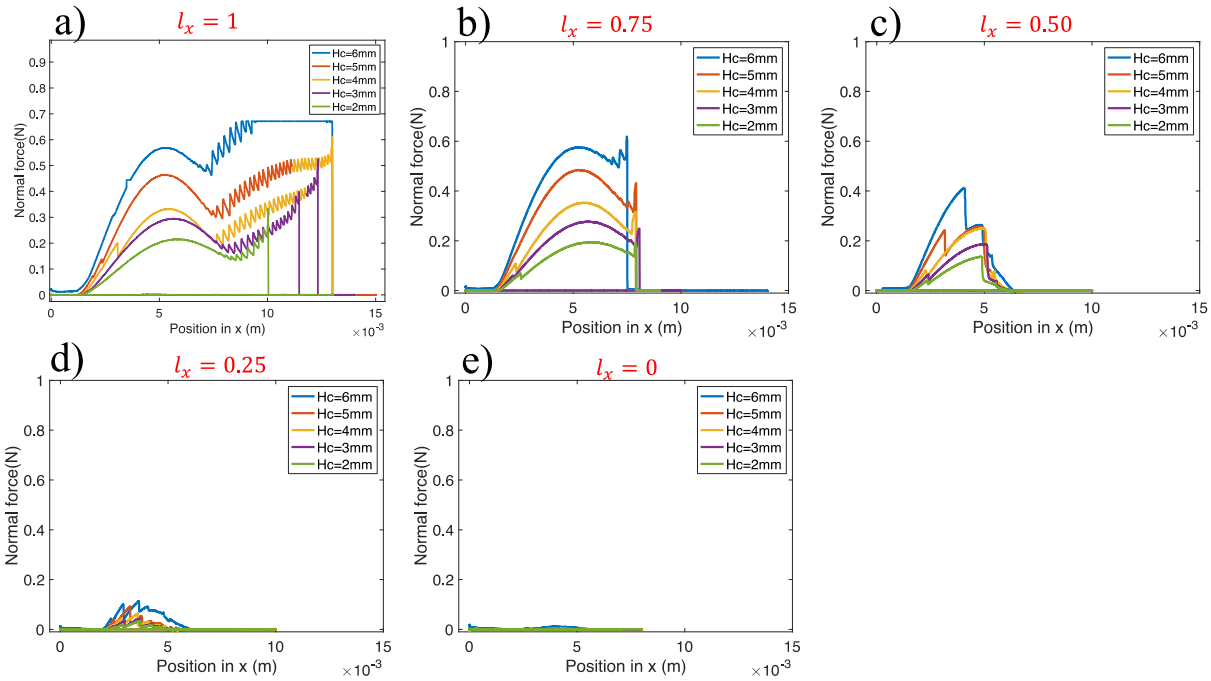

Figure S10. Single pillar data for pillar height= 6 mm and diameter = 3 mm.

Variation of Normal force vs displacement in sliding direction for different diametric overlaps and height of contact. (a) 100% diametric overlap, $l_x = 1$ (b) $l_x = 0.75$ (c) $l_x = 0.50$ (d) $l_x = 0.25$ (e) $l_x = 0$.

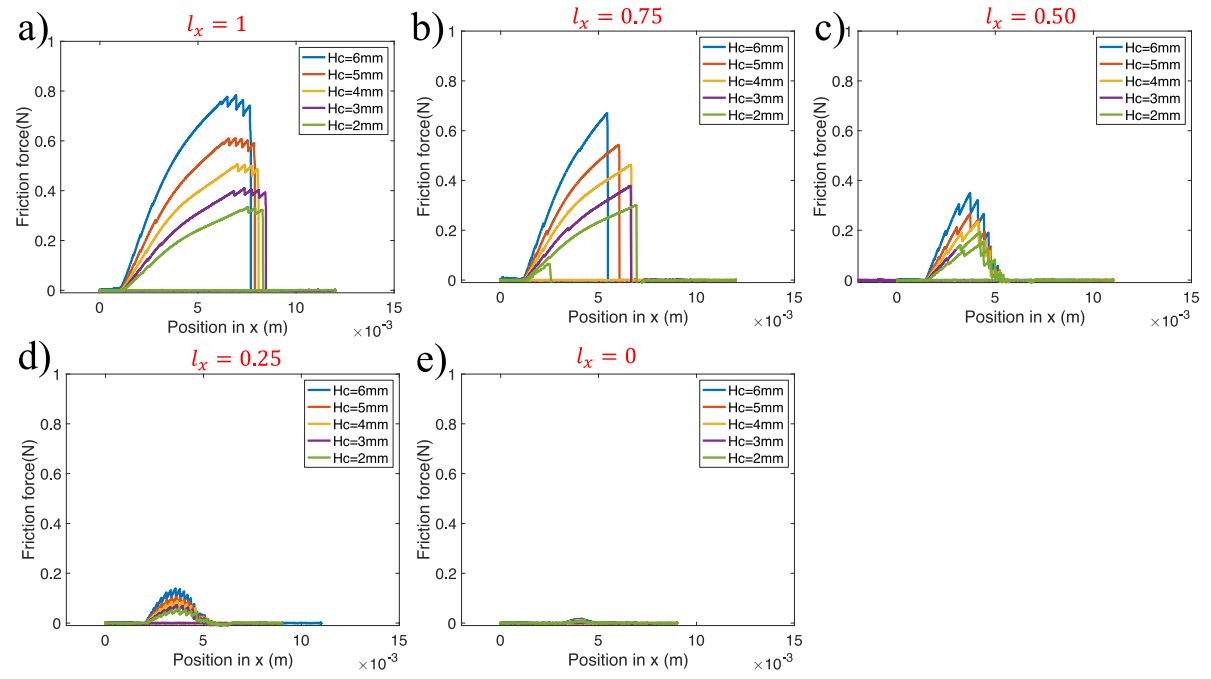

Figure S11. Single pillar experiments (pillar height= 6mm and diameter= 3mm) with silicone oil as lubricant.

Variation of Shear force with displacement for different diametric overlaps and height of contact. (a) 100% diametric overlap, $l_x = 1$ (b) $l_x = 0.75$ (c) $l_x = 0.50$ (d) $l_x = 0.25$ (e) $l_x = 0$.

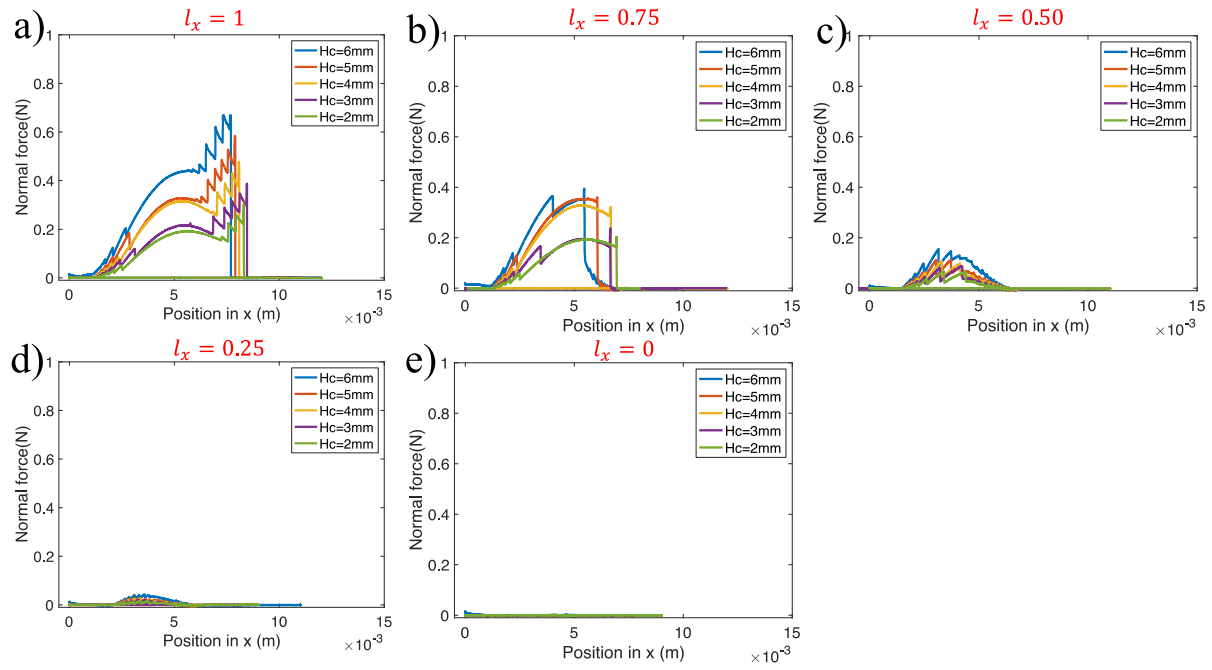

Figure S12. **Single pillar experiments (pillar height= 6mm and diameter= 3mm) with silicone oil as lubricant.**

Variation of Normal force vs displacement in sliding direction for different diametric overlaps and height of contact. (a) 100% diametric overlap, $l_x = 1$ (b) $l_x = 0.75$ (c) $l_x = 0.50$ (d) $l_x = 0.25$ (e) $l_x = 0$.

Comparing single pillar experiments with aspect ratio = 2, with and without lubricant in figure S13 a) to e). Here, shear force for both the experiments is compared and we can see shear force for both the experiments are not that different and have similar peak force, which allows us to neglect adhesion in our model.

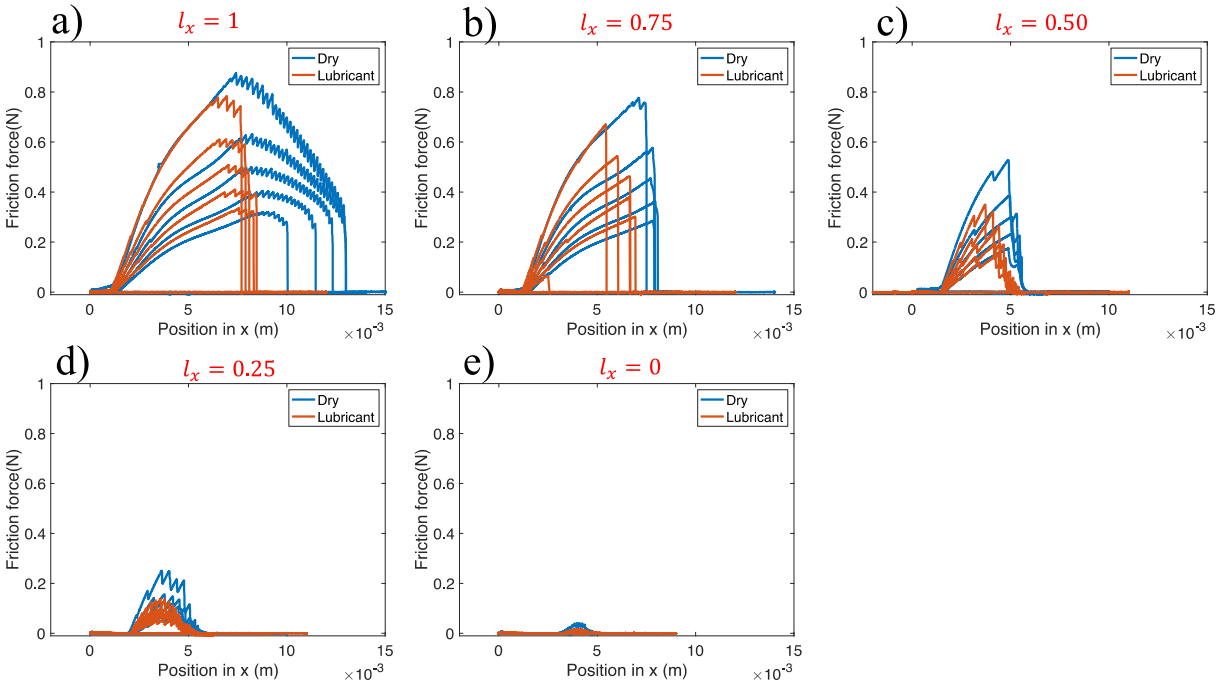

Figure S13. **Comparison of shear force for single pillar experiments with and without silicone oil (pillar height = 6mm, diameter =3 mm).**
Variation of Shear force with displacement for different diametric overlaps and height of contact. (a) 100% diametric overlap, $l_x = 1$ (b) $l_x = 0.75$ (c) $l_x = 0.50$ (d) $l_x = 0.25$ (e) $l_x = 0$.

Figure S14a shows how shear force varies with displacement for different heights of contact and 100% diametric overlap in single pillar experiments with colored squares as fits. Figure S14b shows how normal force varies with displacement for different heights of contact and 100% diametric overlap in single pillar experiments with colored squares as fourth order fits. Figures S14c-h show fits for shear force and normal force at various diametric overlaps, $l_x = 75\%$, 50%, 25%, 0%. (Video **V21_Singlefiber_6mm_100%O_siliconeoil.avi** shows single pillar experiment with silicone oil as a lubricant,**).**

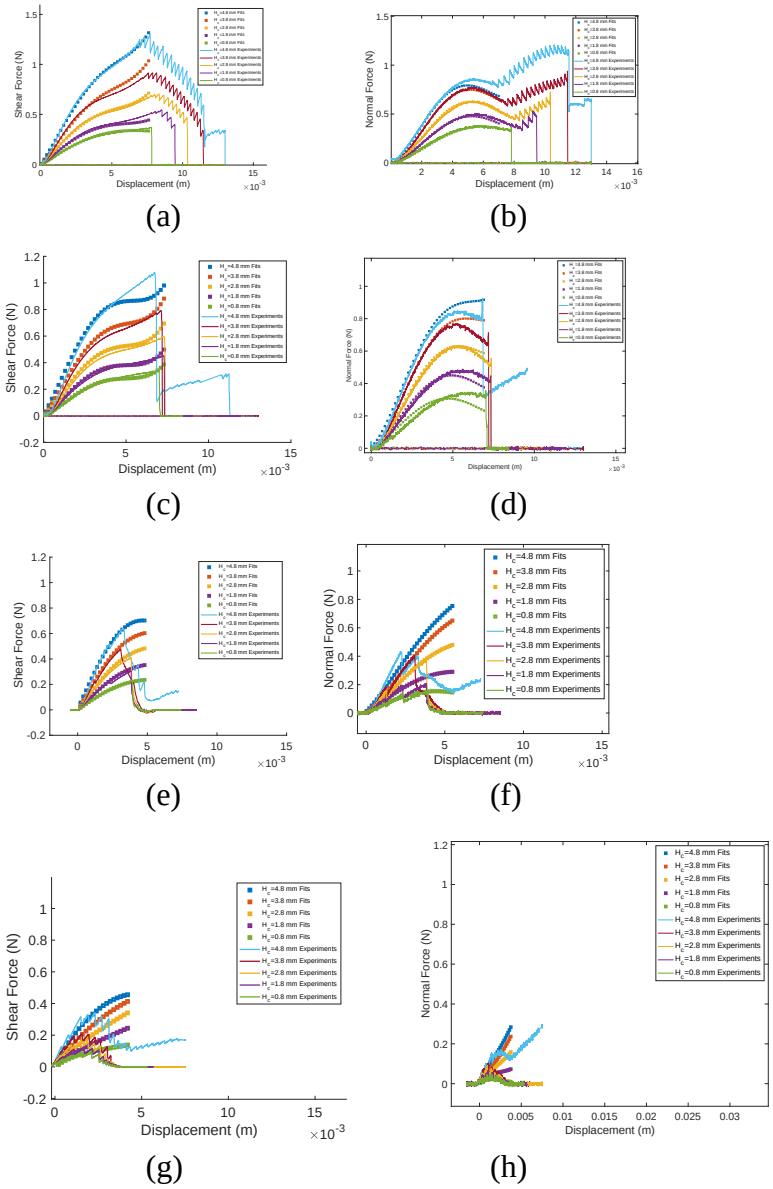

Figure S14. Performing quartic fits for single pillar friction data

(a) Shear force as a function of displacement for 100% overlap, $l_x = 1$. (b) Normal force as a function of displacement for 100% overlap, $l_x = 1$. (c) Shear force as a function of displacement for 75% overlap. (d) Normal force as a function of displacement for 75% overlap. (e) Shear force as a function of displacement for 50% overlap. (f) Normal force as a function of displacement for 50% overlap. (g) Shear force as a function of displacement for 25% overlap. (h) Normal force as a function of displacement for 25% overlap.

Contour plots for four fitting coefficients for shear and normal force are provided in Figure S15. Each contour plot gives a surface function for a fitting parameter. Figure S15a describes contour plots for shear force parameters at different heights and overlaps. Figure S15b describes contour

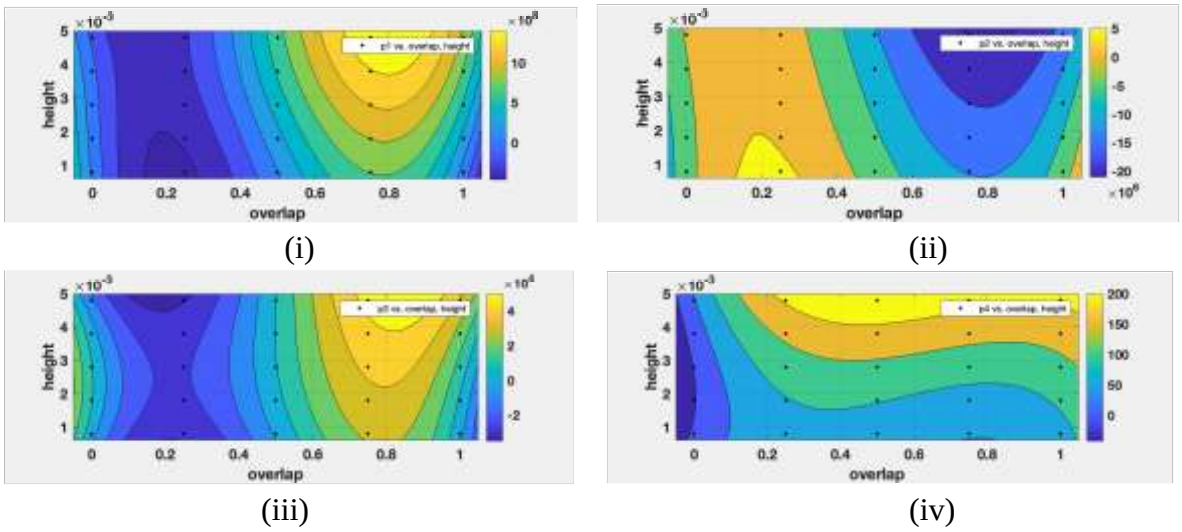

Figure S15. a) Contour plots for four shear force constants

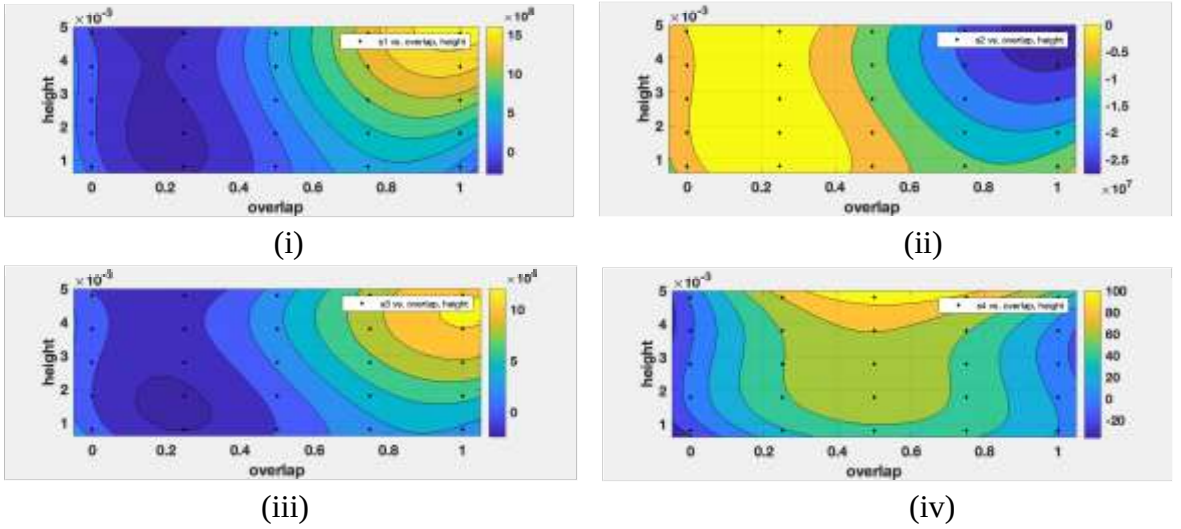

Figure S15. b) Contour plots for four normal force constants

plots for normal force parameters at different heights and overlaps.

S4. Equivalence of Summation of Forces and an Energy Argument to Estimate Friction.

1D Edge Dislocation:

First, we consider a simple case in which the two pillar arrays are perfectly aligned but have different lattice spacing in one direction. This results in the formation of an array of edge dislocations, and we derive the relationship between macroscopic friction and interaction of pairs of pillars. We do so in two ways: (a) by summing up forces and, (b) by an energy argument; we show that the result is the same.

Consider Fig S16 which shows two lattices colored blue and red. The lattices are in perfect orientational alignment, with 100% overlap. The lower blue lattice has pillars in a square array with lattice spacing of a_l in both directions. The upper red lattice has the same lattice parameter in the '*x*' direction but a different lattice parameter in the '*y*' direction:

$$a_u = (1+\varepsilon)a_l \tag{S1}$$

The displacement between red and blue pillars is

$$u = n(a_u - a_l) = n\big((1+\varepsilon)a_l - a_l\big) = \varepsilon n a_l = \varepsilon x \tag{S2}$$

In particular when the displacement becomes a_u, then the corresponding spacing x^* is the period of the edge dislocation array.

$$x^* = a_u/\varepsilon \tag{S3}$$

The shear force on a pillar is a function of overlap and displacement.

$$T = T(u) = T(\varepsilon x) \tag{S4}$$

The local frictional stress is this shear force divided by the unit cell area

$$\tau = \frac{T}{a_l a_u} \tag{S5}$$

which is a function of x. The average friction stress is then given by

$$\tau_{av} = \frac{\int_0^{x^*} T(x)dx}{a_l a_u x^*} \tag{S6}$$

Using (S3) and changing variables to *u* using (S2) we get

$$\tau_{av} = \frac{\int_0^{u^*} T(u)du}{a_l a_u^2} = \frac{w}{a_l a_u^2} \tag{S7}$$

That is, macroscopic friction stress equals energy lost by each pillar in one loading cycle per unit cell area per frictional sliding distance of a_u. In fact, we can more directly obtain (S6) by an energy argument as follows. Imagine relative sliding of one surface with dimensions $L_x, L_y \gg b_u$ over the other by a distance of a_u in the 'y' direction. The state of the interface is identical to

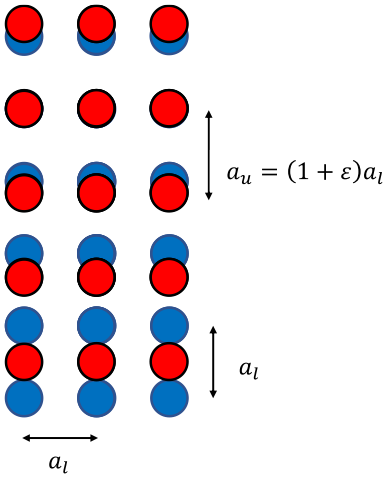

Figure S16. Red and blue arrays of pillars with mismatch in lattice parameter along the 'y' direction. This leads to the formation of edge dislocations.

when the sliding was started, i.e., each pillar has gone through a full loading cycle and dissipates energy of

$$n_x n_y w = \frac{L_x L_y w}{a_l a_u} = \tau_{av} L_x L_y a_u \; ;$$

$$\tau_{av} = \frac{w}{a_l a_u^2} \tag{S8}$$

This simple calculation serves to demonstrate that the summation of forces is equivalent to summation of energy loss per pillar.

S5: Relationship between Moire' patterns, dislocation arrays, and Burgers vectors

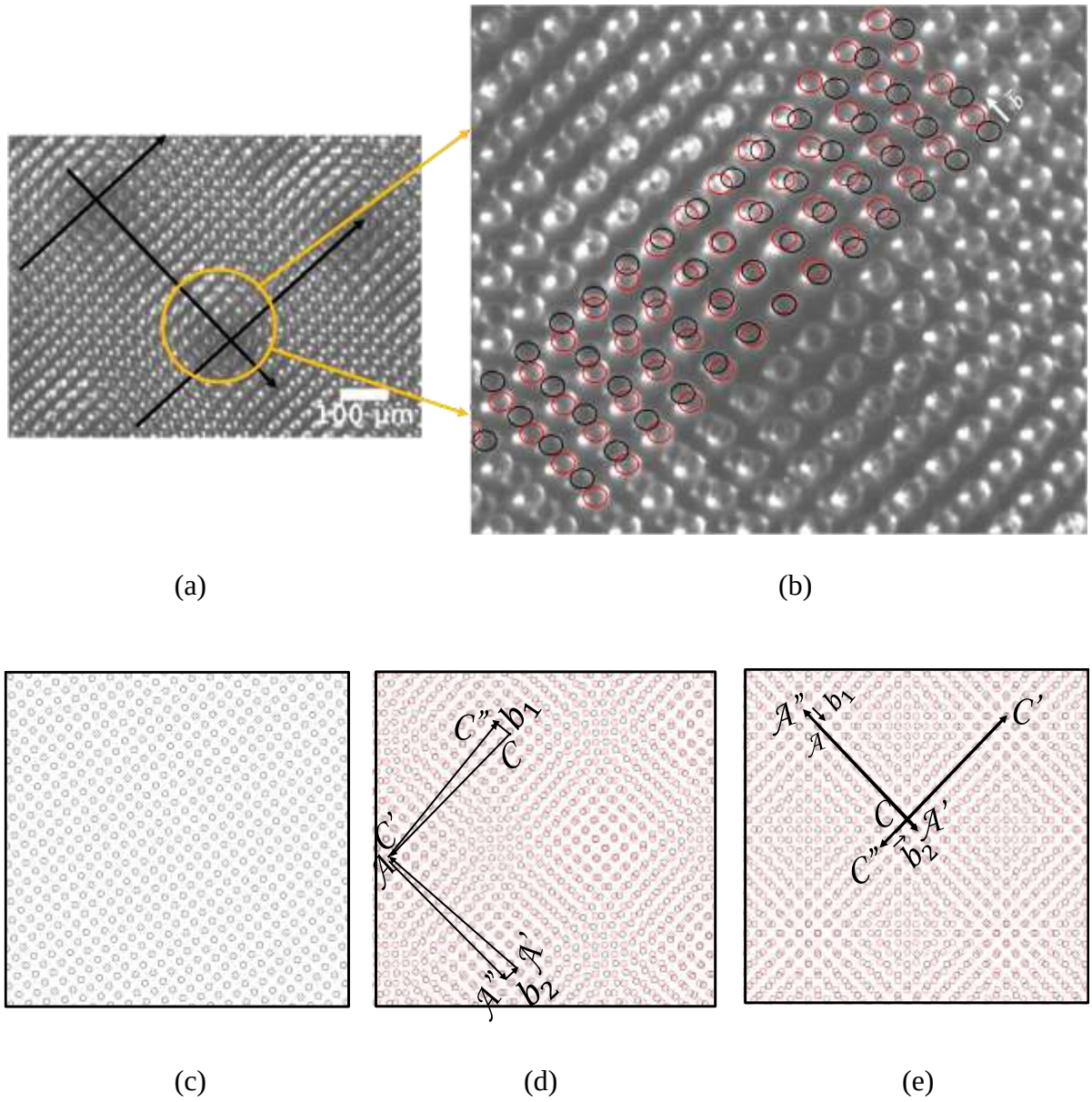

Figure S17. Geometric representation of dislocations and Burgers vector

(a) Optical image of pillar interface: screw dislocations at misorientation, θ = 5°, $\lambda = 1$, (b) Zoomed in version of image showing overlapping pillars on top and bottom samples (black and red circles). Burgers vector is parallel to the dislocation line. (c) Black square lattice representing the bottom sample (d) Black and red lattice at overlapping at misorientation, θ = 5°, λ=1.0, producing screw dislocations. Burgers vector ($\vec{b}_1$) is associated with dislocation line AA'' and runs parallel to it. (e) Black and red lattice at lattice mismatch, λ=1.2, & θ = 0°, producing edge dislocations. Burgers vector ($\vec{b}_1$) is associated with dislocation line $C'C''$ and runs perpendicular to it.

A closer look at the interface (Figs. S17a, b) helps to understand better how we assign screw or edge character to a dislocation. Observe in Fig. S17b (zoomed in figure S17a.), how the relative locations of the red and black circles change as one traverses along a line of pillars. To explain graphically how orientational disregistry gives rise to screw dislocations and lattice parameter mismatch to edge dislocations, consider a black square lattice (Fig. S17c). Now, a red square lattice is put on top of black lattice and rotated by 5° -- a Moiré pattern appears (Fig. S17d). A circuit is made around a dislocation line in a clockwise direction (Fig. S17d), starting with each step of the circuit connecting red lattice sites and going back to the initial point by connecting black lattice sites. When this Burgers circuit is completed, it fails to fully close on itself and the vector linking the end of the circuit to the starting point is the Burgers vector. The Burgers vector can be thus obtained by moving from point A' to point A in the bottom sample (black), and from point A to point A" in the top sample (red) as in Figure S17d. It is evident that the Burgers vector is $\bar{b}_1 = CC"$ and $\bar{b}_2 = A"A'$ for screw dislocations in Fig. 4d and in Fig. S17e, $\bar{b}_1 = AA"$ and $\bar{b}_2 = CC"$ for edge dislocations. (The Burgers vector for a screw dislocation is parallel to the dislocation line and for an edge dislocation it is perpendicular to the dislocation line as in Fig S17d and S17e.)

S6: Model for an edge dislocation in a shape complementary pillar interface.

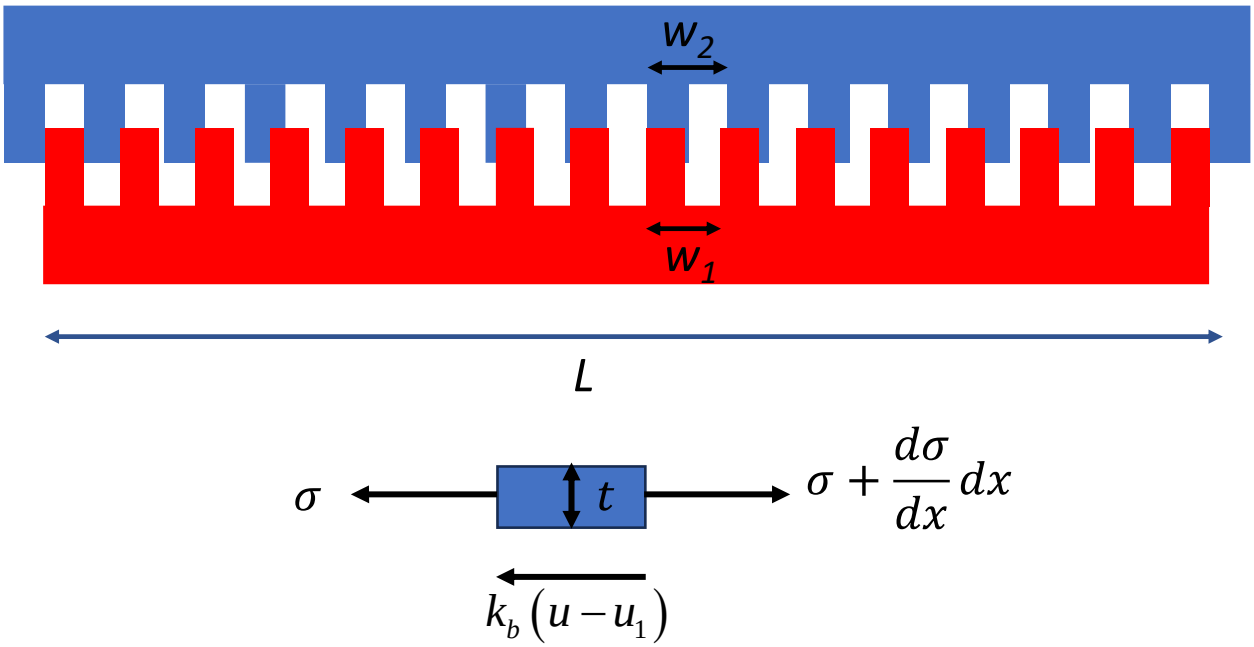

Figure S18. Schematic drawing of a patterned shape-complementary interface with a small difference in period of the pattern which is accommodated by periodic edge dislocations.

Consider Figure S18 in which two patterned surfaces are pressed into each other. The pattern period is slightly different:

$$w_2 = (1+\varepsilon)w_1 = \lambda w_1;\ \lambda \geq 1 \tag{S9}$$

Thus, if we start with a pillar pair where the pillar on one side perfectly matches the channel on the other, then at a length *L* the interface accumulates enough mismatch to equal the period w_1. The system there spontaneously introduces a dislocation, and the mismatch is reset to zero. This period of the array of dislocations, *L,* is given by

$$\begin{aligned} &(n+1)w_1 = nw_2 \Rightarrow (n+1) = n\lambda \\ &\Rightarrow n = 1/(\lambda-1) = 1/\varepsilon \\ &L = nw_1 = w_1/(\lambda-1) = w_1/\varepsilon \end{aligned} \tag{S10}$$

where *n* is the number of pillars in period *L.* Now, the mismatch between the lower and upper parts of the interface is accommodated by a combination of shear and stretch or compression in the plane. In the limit where the pillars are very compliant, all the shear mismatch is in the pillars, and this is a linearly increasing function of *x* between *0* and *L*. This is the situation for the experiments reported in this paper. In the limit where the pillars are very stiff, the pillars do not bend and all the mismatch is accommodated by in-plane deformation.

To see this more concretely, consider a force balance as shown in Fig. S18 where σ is the uniaxial stress, *u* is the in-plane displacement, u_1 is the mismatch of the pillars, and *t* is the thickness of the sample. Force balance in *x* gives

$$t\frac{d\sigma}{dx} - k_b(u-u_1) = 0 \tag{S11}$$

where k_b is the shear stiffness of the layer of pillars and u_1 is

$$u_1 = w_1 \frac{x}{L} \tag{S12}$$

Replacing σ by $E\frac{du}{dx}$, where E is the Young's modulus, we get

$$Et\frac{d^2u}{dx^2} - k_b\left(u - w_1\frac{x}{L}\right) = 0 \tag{S13}$$

Normalize as

$$\begin{aligned} &\bar{u} = u / w_1; \\ &\alpha^2 = \frac{k_b L^2}{Et} \\ &\bar{x} = x / L; \\ &\bar{\sigma} = \frac{\sigma L}{E w_1} = \frac{d\bar{u}}{d\bar{x}} \end{aligned} \tag{S14}$$

to get

$$\frac{d^2\bar{u}}{d\bar{x}^2} - \alpha^2\left(\bar{u} - \bar{x}\right) = 0 \tag{S15}$$

Its solution is

$$\bar{u} = \bar{x} + A\cosh\left(\alpha\bar{x}\right) + B\sinh\left(\alpha\bar{x}\right) \tag{S16}$$

The boundary condition at $\bar{u}\left(\bar{x}=0\right)=0$ implies that A=0. The second boundary condition is

$$\begin{aligned} &\bar{\sigma}\left(\bar{x}=1\right)=0; \frac{d\bar{u}}{d\bar{x}}\left(\bar{x}=1\right)=0 \\ &B = -\frac{1}{\alpha\cosh\left(\alpha\right)} \end{aligned} \tag{S17}$$

So that the solution is

$$\begin{aligned} &\bar{u} = \bar{x} - \frac{\sinh\left(\alpha\bar{x}\right)}{\alpha\cosh\left(\alpha\right)} \\ &\bar{\sigma} = \frac{d\bar{u}}{d\bar{x}} = 1 - \frac{\cosh\left(\alpha\bar{x}\right)}{\cosh\left(\alpha\right)} \end{aligned} \tag{S18}$$

Consider the limit $\alpha \to 0$, where the beam is compliant.

$$\begin{aligned} &\bar{u} \to 0; \\ &\bar{\sigma} \to 0. \end{aligned} \tag{S19}$$

This is the limit in our experiments. If $\alpha \to \infty$, the beam is stiff compared to the backing, then for locations far from the dislocation, which brings the pillars into perfect registry.

$$\begin{aligned} &\bar{u} \to \bar{x}; \\ &\bar{\sigma} \to 1. \end{aligned} \tag{S20}$$

The foregoing serves to illustrate how the pillar-pillar interface can exhibit both limits, the one reported in this paper and the one that is closer to that commonly found in crystalline boundaries.

Videos

1. **V1_lambda=1_0_deg.avi:** This video shows an interface of pillars at $\lambda = 1$, $\theta = 0°$ at a 5x magnification and 0.5V/0.0745N normal load.
2. **V3_lambda=1_5_deg_ ScrewDislocation.avi:** This video shows an interface of pillars at $\lambda = 1$, $\theta = 5°$ at a 5x magnification and 0.5V/0.0745N normal load.
3. **V8_lambda=1.023_0deg_EdgeDislocation:** This video shows an interface of fibrils at $\lambda = 1.023$, $\theta = 0°$ at a 2x magnification.
4. **V10_lambda=1.023_5_deg_MixedDislocation.avi:** This video shows an interface of fibrils at $\lambda = 1.023$, $\theta = 5°$ at a 5x magnification and 0.5V/0.0745N normal load.
5. **V19_Singlefiber_4.8mm_100%O:** This video shows single pillar pair experiment (aspect ratio=1.6) at 100% diametric overlap and 4.8 mm as the height of contact.
6. **V20_singlefiber_6mm_100%O:** This video shows single pillar pair experiment (aspect ratio=2) at 100% diametric overlap and 6 mm as the height of contact.
7. **V21_Singlefiber_6mm_100%O_siliconeoil:** This video shows single pillar pair experiment (aspect ratio=2) at 100% diametric overlap and 6 mm as the height of contact with silicone oil.

[1] Z. He, Z. Liu, M. Li, C. Y. Hui, and A. Jagota, "Meso-scale dislocations and friction of shape-complementary soft interfaces," *J R Soc Interface*, vol. 18, no. 175, p. 20200940, Feb 2021, doi: 10.1098/rsif.2020.0940.